



Full Text View

[Volume 32, Issue 3 \(March 2002\)](#)

Journal of Physical Oceanography

Article: pp. 957–972 | [Abstract](#) | [PDF \(1.29M\)](#)

The Alongshore Transport of Freshwater in a Surface-Trapped River Plume^{*}

Derek A. Fong

Massachusetts Institute of Technology/Woods Hole Oceanographic Institution Joint Program in Oceanography, Woods Hole, Massachusetts

W. Rockwell Geyer

Department of Applied Physics and Engineering, Woods Hole Oceanographic Institution, Woods Hole, Massachusetts

(Manuscript received November 6, 2000, in final form August 2, 2001)

DOI: 10.1175/1520-0485(2002)032<0957:TATOFI>2.0.CO;2

ABSTRACT

The alongshore transport of a surface-trapped river plume is studied using a three-dimensional model. Model simulations exhibit the previously observed rightward veering (in the Northern Hemisphere) of the freshwater and establishment of a downstream geostrophically balanced coastal current. In the absence of any ambient current, the plume does not reach a steady state. The downstream coastal current only carries a fraction of the discharged freshwater; the remaining fraction recirculates in a continually growing “bulge” of freshwater in the vicinity of the river mouth.

The river mouth conditions influence the amount of freshwater transported in the coastal current relative to the growing bulge. For high Rossby number [$O(1)$] discharge conditions, the bulge shape is circular and the coastal current transport is smaller than for the model runs of low Rossby number discharges. For all model runs conducted without an ambient current, the freshwater transport in the coastal current is less than the freshwater discharged at the river mouth.

The presence of an ambient current (in the same direction as the geostrophic coastal current) augments the transport in the plume such that its downstream freshwater transport matches the freshwater source, and the plume evolves to a steady-state width. The steady-state transport accounted for by the ambient current is independent of the strength of the ambient current. The amplitude of the ambient current only determines the time required to reach a steady-state plume width. A key result of this study is that an external forcing agent (e.g., wind or ambient current) is required in order for the entire freshwater volume discharged by a river to be transported downstream.

Table of Contents:

- [Introduction](#)
- [The numerical model](#)
- [The unforced river plume](#)
- [The influence of an ambient](#)
- [Summary](#)
- [REFERENCES](#)
- [TABLES](#)
- [FIGURES](#)

Options:

- [Create Reference](#)
- [Email this Article](#)
- [Add to MyArchive](#)
- [Search AMS Glossary](#)

Search CrossRef for:

- [Articles Citing This Article](#)

Search Google Scholar for:

- [Derek A. Fong](#)
- [W. Rockwell Geyer](#)

1. Introduction

The anticyclonic turning of large-scale river inflow ([Garvine 1995](#)) in the Northern Hemisphere has been well documented in previous studies. The freshwater discharged from the Chesapeake and Delaware Bays and Androscoogin/Kennebec Rivers have all been found to leave a significant freshwater signature toward the right and downstream of the river mouth (where downstream is defined to refer hereafter to the direction a Kelvin wave propagates) ([Boicourt 1973](#); [Münchow and Garvine 1993a](#); [Fong et al. 1997](#)). Similar behavior has also been observed in the laboratory ([Griffiths and Hopfinger 1983](#); [Stern et al. 1982](#); [Whitehead and Chapman 1986](#)) and in numerical models ([Kourafalou et al. 1996](#); [Oey and Mellor 1993](#); [Chao and Boicourt 1986](#)).

Based on numerical modeling studies, the plume can be separated into two dynamically distinct regions: a bulge region near the river mouth and a downstream coastal current ([Chao and Boicourt 1986](#)). Many of the previous studies (e.g., [Kao 1981](#)) have focused primarily on the downstream coastal current; these studies have found that the coastal current is largely in geostrophic balance. This cross-shore momentum balance is consistent with field observations ([Münchow and Garvine 1993b](#)).

A few studies have looked at the dynamics at the river mouth ([Valle-Levinson et al. 1996](#); [Zhang et al. 1987](#); [Chao and Boicourt 1986](#)). These papers investigate the exchange flows near the estuary/river mouth and the lateral variations in the estuarine circulation for a wide estuary/river mouth. Less attention has been paid to the bulge region itself, which appears to be a prominent feature in previous numerical investigations (e.g., [Oey and Mellor 1993](#); [Chao and Boicourt 1986](#)) but is less documented in the observations.

The plume bulges observed in models are usually more pronounced than those in nature. For example, observations of the surface salinity structure of the Chesapeake plume ([Boicourt 1973](#)) suggest a slight bulge near the river mouth; however, the downstream coastal current is nearly the same width as the bulge, in contrast to [Chao and Boicourt's \(1986\)](#) simulation. [Masse and Murthy \(1992\)](#) observe a fairly pronounced bulge that is three times the width of the coastal current but nowhere near the factor of 8 difference observed in a recent numerical study by [Garvine \(2001\)](#).

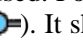
[Yankovsky and Chapman \(1997\)](#) distinguish between the bulge and coastal current for a surface-trapped river plume. They suggest that the dynamics within the bulge are primarily cyclostrophic in nature; that is, the momentum balance is dominated by the pressure gradient, the Coriolis force, and the centrifugal force associated with the azimuthal velocity around the bulge. Their analysis, however, assumes that the plume is in steady state. It is likely, however, that the plume is not in steady state. Both [Oey and Mellor \(1993\)](#) and [Chao and Boicourt \(1986\)](#) simulations show a bulge that appears to grow in time.

Another issue that makes the comparison of field observations and numerical modeling studies of river plumes difficult is the time variability of the buoyancy forcing in nature. This may make it difficult to directly compare with steady numerical results. Differences are further confounded by the presence of forcing due to ambient alongshore currents, which are present on many continental shelves.

The experiments presented in this study investigate the dynamics of the bulge and explain how its persistence and growth are ultimately related to the alongshore freshwater transport in the coastal current. In particular, this study demonstrates that the frequently observed differences in the bulge between idealized numerical experiments and field observations are due to external forcing in the latter. Furthermore, it will be shown that an ambient current of any magnitude (in the direction of Kelvin wave propagation) reconciles the difference in plume structure between models and field observations; the ambient current is sufficient to arrest bulge growth. Despite being highly idealized, the numerical experiments presented help elucidate some of the important dynamics associated with an unforced surface-trapped plume and demonstrate the consequences of an ambient current, or lack thereof, on the freshwater transport.

The paper is organized as follows. In [section 2](#), the numerical model is presented. The dynamics of the unforced river plume are investigated in [section 3](#), concentrating on the implications for the alongshore transport of freshwater. The influence of an ambient alongshore flow on both plume structure and freshwater transport is considered in [section 4](#). The results are summarized in [section 5](#).

2. The numerical model

A three-dimensional, primitive equation model ([Blumberg and Mellor 1987](#)) [Estuarine Coastal Ocean Model-3D (ECOM-3D)] is used. For simplicity, the model domain is chosen to consist of a rectangular basin with a flat bottom of 50-m depth ([Fig. 1](#) ). It should be noted that changing the depth of the domain did not change the qualitative results presented herein, nor did the quantitative results change appreciably. Likewise, a simple source configuration is used to represent the river mouth. Freshwater is discharged uniformly (in y and z) at the coastline ($x = 0$) via a river centered at $y = 277$ km into a 65

km × 340 km model basin. Use of a simple estuary source (see [Fong and Geyer 2001](#)) did not have any appreciable effect on the solutions.

In order to resolve the spatial structure of the plume, a variable resolution grid with $50 \times 100 \times 23$ grid cells is employed (shown as dots in [Fig. 1](#)). The horizontal grid resolution is 1.5–3 km in the cross-shore direction and 3–6 km in the alongshore direction; vertical grid resolution is less than 1 m within the surface-trapped plume.

The model solves the hydrostatic, Boussinesq primitive equations. Subgrid-scale processes are parameterized by eddy coefficients for both momentum and scalar diffusion using the Mellor–Yamada level 2.5 closure scheme ([Mellor and Yamada 1982](#)) for vertical mixing. Horizontal diffusivities are held constant at $10 \text{ m}^2 \text{ s}^{-1}$. At this value, it is found to have little influence on the plume behavior and dynamics. The influence of rotation is implemented with a constant Coriolis parameter f set to 10^{-4} s^{-1} , a reasonable value for a midlatitude plume. The model uses a split time step for internal and external modes. The external mode is two-dimensional and stepped in 10-s steps to satisfy the (CFL) condition associated with surface gravity waves. The internal-mode time step, based on the internal wave speed, is 7 min. A recursive Smolarkiewicz ([Smolarkiewicz and Grabowski 1990](#)) scheme is used to advect scalar fields. General model properties and details of the numerical algorithms can be found in [Blumberg and Mellor \(1987\)](#).

The model is forced with a river inflow centered at $y = 287.5 \text{ km}$. The river inflow is of uniform density and discharged with uniform velocity from a river mouth of width L_r and depth h_r .

This buoyancy forcing is steady and occurs for a period of up to 30 days. For the model runs investigating the role of ambient flows, a uniform barotropic alongshore ambient flow field is imposed at the upstream ($y = 340 \text{ km}$) boundary of the model domain. All model runs presented neglect the influence of tides and winds. The only variable scalar property considered in this study is salinity. The temperature of both the river discharge and the ambient coastal water is held fixed at 4°C . The ambient coastal salinity S_0 is 32 psu, while the salinity of the river inflow ranges from 16 to 28 psu.

It is worth noting that rarely in nature does a river plume develop in the absence of either winds or an ambient flow field for more than a few days, so these simulations are not intended to represent actual river outflows. The goal of this study is, however, to understand the freshwater transport and plume structure resulting from the buoyancy flux itself and to elucidate how these characteristics are modified in the presence of a simple ambient flow field.

3. The unforced river plume

Four model parameters are varied within the following ranges: the volume flux of water discharged by the river, $2500 < Q_r < 10\,000 \text{ m}^3 \text{ s}^{-1}$; the density anomaly of the river discharge, $3.1 < (\Delta\rho)_r < 12.4 \text{ kg m}^{-3}$, which is equivalent to a salinity anomaly of the river discharge $4 < (\Delta S)_r < 16 \text{ psu}$; the width of the river inflow, $3 < L_r < 30 \text{ km}$; and the thickness of the river inflow, $3 < h_r < 30 \text{ m}$. For all cases presented, the equivalent freshwater discharged by the river is $Q_{\text{fr}} = 1250 \text{ m}^3 \text{ s}^{-1}$, where

$$Q_{\text{fr}} = Q_r \frac{(\Delta S)_r}{S_0}.$$


[Table 1](#) summarizes the inflow parameters for all the model runs.


For the narrowest river mouth cases considered ($L_r = 3 \text{ km}$), the river mouth is only one model grid cell wide. To insure that the results presented were not dependent on the under-resolution of the river mouth, sensitivity tests were conducted using a limited model domain at four times the horizontal resolution (for both x and y directions, or 0.375 and 0.75 km, respectively) of the standard runs reported. The basic properties of bulge width and position, coastal current width, and freshwater transport agree to within 2%. However, there was a noticeable change in the plume structure at the bulge circumference between the low and high resolution simulations. The wavelike meanders surrounding the bulge in [Fig. 2](#) disappeared in the high resolution simulation. This discrepancy suggests that in order to model the detailed dynamics of the bulge region, and the potential eddy fluxes associated with it (e.g., [Oey and Mellor 1993](#)), one must be careful in choosing the grid resolution of the model. Nonetheless, given the agreement between the high resolution and standard resolution runs, all the results presented in this study were conducted at the standard resolution.

a. Base case


As a base case (run 1 in [Table 1](#)), a freshwater river inflow of $1250 \text{ m}^3 \text{ s}^{-1}$ [accomplished with a $10\,000 \text{ m}^3 \text{ s}^{-1}$

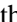
discharge of 28 psu salinity ($\Delta\rho = 3.1 \text{ kg m}^{-3}$) is imposed entering a coastal ocean initially at 32 psu salinity. The freshwater enters through a river mouth of 3-km width and 15-m depth. The magnitude of the freshwater inflow is representative of a moderately strong discharge during the spring freshet for several North American rivers such as the Kennebec/Androscoggin, Delaware, and the South Atlantic Bight river systems ([Fong et al. 1997](#); [Münchow and Garvine 1993b](#); [Blanton and Atkinson 1983](#)).

The development of the unforced plume closely resembles the behavior found in previous modeling studies (e.g., [Oey and Mellor 1993](#); [Chao 1998](#)) of surface-trapped plumes. Most of the river water turns to the right upon entering the model domain ([Fig. 2](#) ) . After only a few days, the plume has developed into two distinct regions, a near-source bulge and a downstream coastal current. The coastal current is only a few kilometers wide, in contrast to the continually expanding bulge region, which extends over 30 km offshore after seven days of river discharge. In addition, there is a small leakage of water upstream, that is, in the direction opposite of Kelvin wave propagation, similar to that found in previous modeling studies such as [McCreary et al. \(1997\)](#) and [Chapman and Lentz \(1994\)](#).


[Chapman and Lentz \(1994\)](#) suggest that the upstream flow is related to the initial geostrophic adjustment of the river discharge. They argue that this produces a buoyancy flux that subsequently feeds a self-sustaining upstream propagation of the upstream intrusion. The simulations presented here are consistent with their hypothesis. The northward intrusion is present at the onset of river discharge and is sustained for all time ([Fig. 2](#) ) . In addition, the model runs conducted in this study exhibit stronger upstream propagation for larger density anomaly inflows, consistent with [Chapman and Lentz \(1994\)](#).

[McCreary et al. \(1997\)](#) found that upstream intrusion of the plume is found in the presence of an ambient stratification in the coastal waters. The northward intrusion observed here and in other studies (e.g., [Chapman and Lentz 1994](#); [Kourafalou et al. 1996](#)) takes place in spite of an initially unstratified coastal ocean. The upstream transport of freshwater in numerical models as a function of different model parameters is investigated in a recent study by [Garvine \(2001\)](#). For the results presented in this study, it is only important to note that the upstream leakage can account for up to 10% of the total freshwater discharge.

The coastal current is unidirectional with velocities up to 40 cm s^{-1} in the downstream direction. The cross-shore momentum balance is primarily geostrophic in the coastal current with the Coriolis and pressure gradient terms being over a magnitude larger than all other terms ([Fig. 3](#) ) .

The bulge region is an anticyclonic gyre with velocities approaching 50 cm s^{-1} at its circumference and slower velocities near the center. The transport around the bulge is not axially symmetric. The seaward side of the bulge has a stronger flow field than near the coast. The asymmetry can be explained by a simple cartoon (see [Fig. 4](#) ) . The perimeter flow on the seaward side of the bulge contains both recently discharged river water and “older” recirculating water. The water that does not get transported in the coastal current is then recirculated in the near-coast portion of the bulge. The freshwater transport in the coastal current Q_{fcc} is defined as

$$Q_{fcc} \equiv \iint v \frac{\Delta S}{S_0} dA,$$

where v is the alongshore velocity, ΔS is the salinity difference between the plume and ambient water, S_0 is the ambient salinity, 32 psu, and the area integral is computed over the depth/cross-shore section of the coastal current. For the base case, the freshwater transport in the coastal current (measured at $y = 252 \text{ km}$) is between 500 and $600 \text{ m}^3 \text{ s}^{-1}$ ([Fig. 2](#) ) , less than half of the $1250 \text{ m}^3 \text{ s}^{-1}$ freshwater input by the river. Since the coastal current does not transport all of the freshwater input at the river mouth, the excess causes the bulge to recirculate and grow. It is unclear a priori whether the time-dependent bulge recirculation is a consequence of the strength of the coastal current or vice versa. The influence of the source conditions on the bulge behavior and freshwater transport in the coastal current will be discussed in [section 3c](#).

The discrepancy between freshwater transport in the coastal current and that input by the river persists throughout the model run; thus the bulge continues to grow. The mismatch between the river discharge and coastal current transport does vary somewhat in time; however the freshwater transport of the coastal current is found to be significantly less than the river discharge for the entire model simulation. The temporal variability of the freshwater transport is discussed in [section 3d](#).

In spite of the observed meanders on the circumference of the bulge region, the bulge remains stable for all 21 days of simulation. In fact, none of the conducted model runs exhibits eddy shedding as predicted by [Oey and Mellor \(1993\)](#). As discussed earlier, it is plausible that the observed instabilities in their modeling study are due to their coarse grid resolution, in addition to their choice of scalar advection scheme.

The continuous growth of the bulge implies that the unforced river plume is an unsteady phenomenon. This behavior contrasts the assumption of steadiness used in several previous studies of freshwater plumes ([Yankovsky and Chapman 1997](#); [Zhang et al. 1987](#); [Garvine 1996](#)).

b. Coastal current freshwater transport

Qualitatively, the freshwater transport in the coastal current can be understood by considering a simple representation of the plume. Consider a two-layer, Margules front system that has a quiescent lower layer and a geostrophic cross-shore momentum; that is,

$$\mathbf{v} = g \frac{\Delta\rho}{\rho_0 f} \frac{\partial h}{\partial x} \quad (1)$$

where $\Delta\rho = (\rho_2 - \rho_1)$ is the density difference between the plume and the ambient water, h is the plume thickness (which can vary as a function of x , the cross-shore direction), \mathbf{v} is the alongshore velocity, f is the Coriolis parameter, ρ_0 is an ambient density equal to 1025 kg m^{-3} , and g is the gravitational acceleration.

The transport in the coastal current is

$$Q_{cc} \equiv \iiint \mathbf{v} \, dA = \int_0^L \mathbf{v} h \, dx, \quad (2)$$

where A is the cross-sectional area of the plume and L is the plume width. Substitution of (1) into (2) and integration gives an expression for the geostrophic transport in the coastal current:

$$Q_{cc} = \frac{g'}{2f} (h_L^2 - h_0^2), \quad (3)$$

where g' is the reduced gravity ($g\Delta\rho/\rho$) and h_0 and h_L are the plume thickness at the coast and its offshore edge, respectively. If one assumes $h_L \ll h_0$, then the transport can be estimated by

$$Q_{cc} = \frac{g'}{2f} (h_0^2), \quad (4)$$

where the minus sign associated with transport being in the negative y direction has been dropped for convenience. It should be noted that, since the density of the plume is only a function of salinity in the numerical experiments, the salinity anomaly is approximately proportional to the density anomaly and, hence, g' (assuming a linear equation of state, $\Delta\rho = \beta\Delta S$, where $\beta = 0.79 \text{ m}^3 \text{ kg}^{-1} \text{ psu}^{-1}$).

Similarly, one can derive an expression for the freshwater transport for the Margules front:

$$Q_{fcc} \equiv \iiint \mathbf{v} \frac{\Delta S}{S_0} \, dA \approx \frac{\rho_0}{g\beta S_0} \frac{(g' h_0)^2}{2f}, \quad (5)$$

where $\Delta\rho_0$ is the ambient water density and, again, it has been assumed that $h_L \ll h_0$. [Equation \(5\)](#) predicts that, for a given latitude (or assuming an f plane) and background salinity, the freshwater transport is a function of only $g' h_0$, the buoyancy of the plume at the coast. This quantity is proportional to the potential energy of the coastal current.

For more complicated salinity structures than a Margules front, the functional relationship between the plume buoyancy and the freshwater transport remains the same. Namely, for a continuously stratified plume, the freshwater transport in the coastal current depends on $(g' h_0)^2$, and only the coefficient in front of expression (5) is modified and g' is based on the depth-averaged density anomaly. For example, for a salinity profile that varies linearly with x and z within the plume [$\Delta S = \Delta S_0(1 - x/L + z/h_0)$, where ΔS_0 is the maximum salinity anomaly within the plume], the factor of one-half in (5) is replaced

c. Plume response for different inflow parameters

In this subsection, the behavior and physics of the base case are tested for a variety of forcing conditions and summarized in [Table 1](#).

1) POTENTIAL ENERGY AND FRESHWATER TRANSPORT IN THE COASTAL CURRENT

For all the model runs conducted, the freshwater transport in the coastal current shows a consistent dependence on the plume's potential energy at the coast. A linear fit of the observed model freshwater transport as a function of the squared potential energy at the coast $(g' h_0)^2$ at $t = 5$ days is shown in [Fig. 5](#). The least squares regression of the model's coastal current freshwater transport,

$$Q_{\text{fcc}} = \gamma \left(\frac{\rho_0}{g\beta S_0} \right) \frac{(g' h_0)^2}{f} + \sigma, \quad (6)$$

results in $\gamma = 0.377$ and $\sigma = 61 \text{ m}^3 \text{ s}^{-1}$. The fit is excellent ($r^2 = 0.94$), consistent with a cross-shore momentum balance that is primarily geostrophic in nature. The computed y intercept σ is small relative to the total transport for most model runs. The regression is similar for the entire duration of the model runs considered. For a regression that includes all model runs for $t = 1$ through $t = 14$ days, the fit is also excellent with $\gamma = 0.383$ and $r^2 = 0.98$. As previously noted, the coefficient γ can be interpreted as a “shape factor” related to the details of the salinity distribution within the coastal current. [Figure 3](#) shows a typical section within the coastal current. The structure is roughly linear in both the depth and cross-shore directions, consistent with the value of $\gamma = 1/3$ for linearly varying salinity in x and z .

2) SOURCE CONDITIONS AND FRESHWATER TRANSPORT IN THE COASTAL CURRENT

For all model runs conducted, the freshwater transport in the coastal current is less than the freshwater supplied by the river. The amount of this mismatch varies according to the forcing conditions at the river mouth. The variability and dependence of the freshwater transport on the river mouth conditions are discussed below.

The above regression analysis indicates that, if the potential energy at the edge of the coastal current were large enough, then all the river transport would be carried downstream by the plume. Using the regression computed from [Eq. \(6\)](#), the value of $g' h_0$ necessary for $Q_{\text{fcc}} = Q_{\text{fr}}$ is $0.279 \text{ m}^2 \text{ s}^{-2}$. In other words, if the potential energy in the coastal current (at $x = 0$) were to equal $0.279 \text{ m}^2 \text{ s}^{-2}$, there would be no mismatch between the coastal current transport of freshwater and the river discharge.

The potential energy for three different model runs (5, 1, and 11) in which there is a significant variation in the coastal current transport is contoured in [Fig. 6](#). Also shown in [Fig. 6](#) are contours of the Bernoulli function, which quantifies the total plume energy:

$$B = g' h + \frac{\bar{u}^2 + \bar{v}^2}{2},$$

where \bar{u} and \bar{v} are the depth-averaged plume velocities.

All three model cases shown in [Fig. 6](#) exhibit similar potential and total energy levels within the bulge. The potential energy $(g' h)$ of some plume water exceeds $0.279 \text{ m}^2 \text{ s}^{-2}$, and significant portions of the plume have total energies (B) larger $0.279 \text{ m}^2 \text{ s}^{-2}$. The distribution of the potential energy $(g' h)$, however, differs substantially for the runs. The highest potential energy water in run 5 is contained in the center of the recirculating bulge. The potential energy of the fluid making its way into the coastal current is considerably less ($g' h < 0.15 \text{ m}^2 \text{ s}^{-2}$). Run 11, which has a wide river mouth and weaker inflow velocities, has almost the same potential energy making it into the coastal current as observed in the near field. The maximum potential energy water is adjacent to the coast and the coastal current contains water of $g' h > 0.2 \text{ m}^2 \text{ s}^{-2}$, compared with a maximum of $\sim 0.3 \text{ m}^2 \text{ s}^{-2}$ in the bulge. Although the transport in the coastal current is not adequate to match the freshwater inflow, it is much larger than the other two runs by virtue of the higher potential energy in the coastal current.

The Bernoulli function distributions shown in [Fig. 6](#) indicate that for all three model runs, a large fraction of the plume water is of sufficient energy for Q_{fcc} to match Q_{fr} {assuming that all or most of the kinetic energy $[(\bar{u}^2 + \bar{v}^2)/2]$ could be converted into potential energy $(g' h)$. The variability in Q_{fcc} observed between the different runs is not due to a lack of energy in the river discharge. Instead, Q_{fcc} is determined by the spatial distribution of energy in the bulge and, subsequently, the energy of the water entering the coastal current.

Corresponding with the variability in coastal current potential energy are distinct changes in bulge shape between the different model runs. When the coastal current is weak, the bulge is circular in shape, resembling the flow field observed for an anticyclonic eddy ([Fig. 6](#), run 5). In contrast, the bulge for the higher transport cases exhibits a semicircular shape ([Fig. 6](#), run 11).

The shape of the bulge and the freshwater transport in the coastal current are found to depend mainly on the velocity of the inflow and the width of the river mouth ([Table 2](#)). High velocity and narrow river mouth discharges have weaker coastal currents. The Rossby number, $Ro = u_r/fL_r$, was found to best characterize the shape of the bulge and the magnitude of the coastal current transport. The dependence of the coastal current transport on Ro is shown in [Fig. 7](#). Runs 15 and 16 have the same river mouth conditions as the base case (run 1); the Coriolis parameter f for these two runs is, however, reduced to $0.5 \times 10^{-4} \text{ s}^{-1}$ and $0.25 \times 10^{-4} \text{ s}^{-1}$, respectively. The freshwater transport for these two runs is computed farther downstream ($y = 232 \text{ km}$) than for runs 1–14 ($y = 252 \text{ km}$) since the alongshore bulge extent is greater. Both alongshore positions used for the calculation are chosen such that they are downstream of the bulge and there is negligible alongshore variability in freshwater transport ($<10 \text{ m}^3 \text{ km}^{-1} \text{ s}^{-1}$).

The semi-log linear regression of Ro with Q_{fcc} , is statistically significant to the 99% confidence interval ($r^2 = 0.79$). The low Ro model runs have larger coastal current transports than the high Ro cases. Furthermore, the bulge shape is qualitatively correlated with the Rossby number ([Fig. 8](#)). The bulge is more circular for high Rossby number discharges (i.e., the center of the bulge is further offshore) and semicircular in shape for low Ro discharges (i.e., the center of the bulge is closer to shore). Note that the width of the plume bulge is much larger for runs 15 and 16 where the Coriolis parameter has been reduced since their “nondimensional scale time (t/f)” is much larger. The total freshwater volume in runs 15 and 16 is, however, comparable to the other runs; the plume is just thinner for the cases of weaker rotation.

The dependence of the bulge shape on the Rossby number suggests that the ratio of inertial length scale (u_r/f) to the width of the river mouth (L_r) sets the trajectory of the river discharge and the shape of the bulge. The extent of the offshore bulge appears to scale with the inertial length scale, but the alongshore extent of the bulge is related to the width of the river mouth. The larger the Rossby number, the larger the offshore dimension relative to the alongshore scale. The farther offshore the center of the bulge is, the smaller the coastal pressure anomaly, and the smaller the quantity of fluid intercepted by the coastal current ([Fig. 6](#)).

The correlation between the shape of the bulge and mismatch between the freshwater transport of the coastal current and the discharge at the river mouth is related to a study by [Nof \(1988\)](#) of a baroclinic eddy colliding with a wall. He uses a nonlinear, layered, analytic model to determine how an eddy interacts with a wall. In the case where only the outer edge of the eddy interacts with the wall, [Nof \(1988\)](#) finds that there is weak leakage from the eddy. When the eddy is closer to the wall, the leakage (i.e., downstream transport in the coastal current) is larger. The leaked fluid is analogous to the coastal current in the plume, and the baroclinic eddy is similar to the plume bulge. When the bulge is semicircular, the freshwater transport in the coastal current is fairly large. This is similar to the case of large wall penetration into the eddy, which results in significant fluid leakage. In comparison, a circular bulge (small wall penetration) coincides with a weak coastal current transport (little fluid leakage).

For the plume problem, the Ro , based on the outflow conditions at the river mouth, sets the amount of the eddy “sliced off” by the coastal wall. For high Ro , most of the eddy remains intact and the bulge is nearly circular in shape; for low Ro , the eddy is nearly sliced in half ([Fig. 6](#), run 11) and the bulge is semicircular. As a consequence, for high Ro conditions, the high potential energy water from the river discharge is trapped in the center of the bulge as opposed to the low Ro runs where the higher potential energy water is adjacent to the coast. For the latter cases, some of the higher potential energy fluid enters the coastal current, and the freshwater transports are higher.



The growing bulge under all forcing conditions demonstrated here is also consistent with the recent work of [Pichevin and Nof \(1997\)](#) on large-scale buoyant discharges on a beta plane. They suggest that a buoyant discharge on an f -plane will have an unbalanced force due to the downstream current that must be compensated for by either shedding eddies or a continually growing eddy near the buoyant source.

[Garvine \(1995\)](#) suggests the Kelvin number, the ratio of the plume width to the baroclinic Rossby radius, as the important



dynamic classification parameter. This is consistent with the trend exhibited in the experiments of this study. The Rossby number description, however, is prognostic since it relies only on information related to the source conditions at the river mouth. [Garvine's \(1995\)](#) classification, although admittedly more robust for real world plumes (which are forced by winds, ambient currents, and tides), has the shortcoming of requiring a priori knowledge of the critical properties of the already developed plume.


d. Temporal variations in freshwater transport



As mentioned earlier, the difference in coastal current transport and source discharge varies in time. These fluctuations are coincident with temporal variations in both plume thickness and density anomaly in the coastal current. Small temporal variations in plume thickness and density anomaly are observed for each of the model runs. These variations result in changes in the potential energy in the coastal current and, hence, temporal variations in freshwater transport in the coastal current. Because the freshwater transport is dependent on the square of the potential energy in the coastal current, small fluctuations in either the density anomaly or plume thickness in the coastal current can result in appreciable changes in coastal current transport. For the model runs conducted, the freshwater transport in the coastal current does not necessarily attain a steady-state value. One potential source of the variability in the coastal current properties may be the unsteady flow field observed at the circumference of the bulge. It is unclear what exact dynamics control the unsteadiness of the bulge flow field. This problem is beyond the scope of this study.




Nevertheless, in spite of the temporal fluctuations in Q_{fcc} , for all the durations over which the different model runs are conducted, the freshwater transport in the coastal current is observed to be in significant deficit with the freshwater supplied by the river. Corresponding with this mismatch is a bulge that grows in time for all the model simulations ([Fig. 9](#) ). If the mismatch in transports was constant and the bulge circular with constant thickness, then one would expect the bulge width to be proportional to the square root of time t (since the bulge's area grows linearly in time under these assumptions). The bulge widths for the different runs shown in [Fig. 9](#)  are roughly proportional to $t^{1/2}$.

4. The influence of an ambient flow field

The addition of a moderate amplitude ambient flow field dramatically alters plume behavior. For a 10 cm s^{-1} ambient current in the same direction as Kelvin wave propagation (all other parameters identical to the base run), the bulge is distorted ([Fig. 10](#) ) from the structure observed in the unforced case ([Fig. 2](#) ). In the presence of an ambient flow, the bulge does not grow offshore indefinitely. For the 10 cm s^{-1} ambient flow field, the bulge reaches a maximum offshore width after approximately four days and stops growing offshore. For later time, the bulge expands only in the downstream direction. This is consistent with [Zhang et al. \(1987\)](#) and [Valle-Levinson et al. \(1996\)](#), who find that the outflow at the estuary mouth has its offshore extent suppressed by an ambient alongshore current.

The finite offshore growth of the bulge is a consequence of the ambient flow field augmenting the freshwater transport within the bulge. As the bulge grows larger (i.e., greater area in the cross-shore/vertical plane), the effect of the ambient current increases. The offshore bulge growth shuts down when the bulge is sufficiently large that the advection of the bulge by the ambient current can augment the freshwater transport where it equals the freshwater discharged at the river mouth ([Fig. 11](#) ).

After the bulge stops growing offshore, it is advected downstream by the ambient current. For any alongshore location within the bulge, the freshwater transport equals the freshwater discharged by the river. For the model run shown in [Fig. 10](#) , the bulge is advected past $y = 252 \text{ km}$ after approximately seven days. For times greater than seven days, the alongshore freshwater transport matches the river discharge at this alongshore location ([Figs. 10, 11](#) ).

For weaker ambient flows, the time to reach steady-state width is longer and the maximum plume width is larger than for stronger ambient currents. Even for an ambient current as small as 1 cm s^{-1} , the plume eventually reaches a steady-state width (after about 17 days). For large ambient flows ($>20 \text{ cm s}^{-1}$), the steady-state plume width is reached in less than two days ([Fig. 12](#) ). The subsequent downstream bulge growth occurs at a rate approximately equal to the velocity of the ambient current. For example, the bulge expands downstream at approximately 10 cm s^{-1} for $t \geq 4$ days for the model run with a 10 cm s^{-1} ambient flow ([Fig. 12](#) ). The plume behavior demonstrated here explains [Yankovsky and Chapman's \(1997\)](#) surface-trapped plume simulation (their [Fig. 10](#) ), which is not precisely circular, as is assumed in their theory. The distorted nature of their bulge is a consequence of the ambient flow field of 4 cm s^{-1} that was imposed.

The influence of an ambient current on the freshwater transport in the plume can be interpreted as a nearly linear superposition of a barotropic current and the baroclinically induced current associated with the buoyancy of the plume. The freshwater transport can be decomposed into its barotropic and baroclinic components,

$$Q_{\text{fcc}} = \underbrace{\iint v_{\text{bt}} \frac{\Delta S}{S_0} dA}_{\text{barotropic transport}} + \underbrace{\iint v_{\text{bc}} \frac{\Delta S}{S_0} dA}_{\text{baroclinic transport}} \quad (7)$$

where \mathbf{v}_{bc} is the baroclinic velocity and \mathbf{v}_{bt} is the barotropic velocity. The barotropic velocity is defined as the mean velocity beneath the plume and is similar in amplitude to the imposed ambient flow strength. The baroclinic velocity \mathbf{v}_{bc} is equivalent to \mathbf{v} in Eq. (2) is the flow field induced by the cross-shore salinity gradients within the plume; \mathbf{v}_{bc} is assumed to vanish beneath the plume.

Decomposition of the transport between its barotropic and baroclinic components shows that the baroclinic transport is largely independent of the amplitude of the ambient flow field (Fig. 13). The barotropic transport approaches its “steady-state contribution” in a much shorter time period for stronger ambient flows. After five days, all model runs greater than 15 cm s^{-1} have reached a steady-state freshwater transport that matches the river discharge at $y = 252 \text{ km}$. The barotropic transport (at $y = 252 \text{ km}$) associated with the ambient flow accounts for over half the freshwater transported by the coastal current for all the ambient flows considered.

The model runs suggest that the discrepancy between the observed plumes and those simulated in previous modeling studies may largely be accounted for by an ambient current in the direction of Kelvin wave propagation that advects the bulge along the coast. Although the model runs presented here do not include the influence of winds or tidal forcing, it is expected that the ambient flow will have an order-one effect on the geometry of the salinity distribution associated with the plume. For the Chesapeake plume's surface salinity distribution in Boicourt (1973), there is a corresponding southwestward ambient flow field of $O(10\text{--}15) \text{ cm s}^{-1}$ (inferred from Boicourt 1973). It is likely that the nearly uniform plume width observed just downcoast of the Chesapeake is explained by the prevailing ambient currents distorting and advecting the bulge in the alongshore direction. On the other hand, recent observations during the Chesapeake Bay Outflow Plume Experiment suggest the presence of a bulgelike recirculation region south of Cape Henry (Marmorino et al. 1999, 2000).

Notwithstanding the Chesapeake hydrography, there are very few large-scale surveys of surface-trapped plumes. Nevertheless, those that exist are consistent with the paradigm of an ambient flow field distorting the bulge so that it exhibits a large region of uniform width. For example, T. M. Sanders (2000, personal communication) has observed a roughly uniform plume width up to 100 km downstream of the Delaware River mouth. Typical ambient currents for this coastal region are $O(10) \text{ cm s}^{-1}$ in the downstream direction (Münchow and Garvine 1993b). Likewise, recent observations by Geyer et al. (2001, manuscript submitted to *Cont. Shelf Res.*) of the Gulf of Maine plume also show a uniformly wide plume during several hydrographic surveys. For this plume system, the ambient currents range from 5 to 15 cm s^{-1} in the downstream direction. Ambient currents in the direction of Kelvin wave propagation are ubiquitous features of continental shelves (Kundu and Allen 1976; Brink et al. 1980; Beardsley and Boicourt 1981). It has been suggested that they are the result of a rectification of coastally trapped waves (Brink 1986; Haidvogel and Brink 1986; Holloway et al. 1989) or larger-scale buoyancy forcing.

For the less common case of ambient flow fields in the direction opposing Kelvin wave propagation, some plume growth is expected in the direction of these opposing currents. Hickey et al. (1998) observe upstream plume growth for the Columbia plume in the presence of “adverse” ambient currents. Likewise, for the Amazon plume, where rotation is less important, an adverse ambient current is effective at pushing plume waters upstream (Lentz and Limeburner 1995). Recent observations of the Chesapeake plume, under weak wind and ambient flow field conditions ($<5 \text{ cm s}^{-1}$), exhibit a distinct bulge and downstream coastal current which is approximately half as wide as the bulge (W. C. Boicourt 2000, personal communication).

5. Summary

This study has shown that, in the absence of an ambient flow field, a surface-trapped river plume will develop a bulge. The bulge is consistent with a deficit in the transport of freshwater in the coastal current relative to the freshwater volume input by the river. For the model runs considered, the bulge continues to grow and the plume does not reach a steady-state.

The freshwater transport is determined by the potential energy of the coastal current at the coastal wall. More energetic coastal currents (i.e., those with greater buoyancy anomaly $g' h$) are capable of transporting larger fractions of the discharged freshwater. The potential energy in the coastal current and, hence, the freshwater transport are found to be principally dependent on the Rossby number associated with the river discharge. The mechanism controlling the magnitude of the coastal current appears to be related to the geometry of the bulge, which in turn determines the magnitude of $g' h$ at the coast. For the wide range of forcing parameters considered in this study, the unforced plume is found not to transport all

of the freshwater discharged by the river in the downstream coastal current.

Many natural plume systems, including the western Gulf of Maine, Eel River, and South Atlantic Bight plumes, have relatively narrow (<5 km wide) river mouths. This study has demonstrated that for these river mouth conditions [$O(1)$ Ro discharges] there will be a significant fraction of freshwater that is not transported in the unforced coastal current. Even for relatively wide river mouths, such as the Chesapeake Bay, most of the outflow occurs through a narrow channel on the right-hand side of the estuary mouth (looking seaward) during peak runoff conditions ([Marmorino and Trump 2000](#)). One might speculate that this type of plume system might also behave like the higher Rossby number cases studied here.

It has been demonstrated that an ambient alongshore flow field can augment the freshwater transport and distort the bulge. For any ambient current in the direction of Kelvin wave propagation, there exists a quasi-steady bulge and maximum plume width. A secondary effect of an ambient flow in the downstream direction is to halt any upstream transport of freshwater. The upstream propagation physics discussed by [Chapman and Lentz \(1994\)](#) and [McCreary et al. \(1997\)](#) may exist in a natural plume system [e.g., The Columbia River ([Hickey et al. 1998](#))]; however, the presence of a moderate amplitude ambient flow in the direction of Kelvin wave propagation is likely to retard the upstream intrusion and force the plume's buoyancy to be transported only downstream.

Plumes in nature rarely are unforced, and plume behavior may be influenced by external forcing agents. This investigation has demonstrated that an ambient current can dramatically modify a plume's structure and freshwater transport characteristics. One would expect that the presence of a downwelling favorable wind would have a similar effect of distorting the bulge and augmenting the downstream freshwater transport of plume water. For example, [Rennie et al. \(1999\)](#) find enhanced plume velocities in the downstream direction for downwelling wind conditions. Because of their sensitivity to external forcing, plumes in nature do not always resemble the idealized, buoyancy-forced plumes studied in previous laboratory and numerical experiments. In many real plumes, the buoyant discharge and its ultimate fate may be strongly influenced by external forcing agents. Winds and ambient currents are likely to dominate the macroscopic behavior of a plume and the alongshore transport of freshwater.

This study has identified an ambient current as a potential means of reaching “steady state” in a plume. It is worth noting that for fairly typical ambient flows of $5\text{--}10\text{ cm s}^{-1}$, the timescale to steady state is several days. For many plume systems found in nature, the correlation timescale for winds is similar or shorter. Coupled with the possible influence of tides, this suggests that plumes are by nature unsteady phenomena, even with a steady outflow. It is worth noting that, though winds have been neglected in this study, they can drive significant coastal currents. Therefore, any study hoping to understand or predict the freshwater transport of a plume needs to consider the influence of both winds and ambient flows.

Acknowledgments

Valuable discussions with D. Chapman, R. Garvine, S. Lentz, and A. Valle-Levinson were of immeasurable value during the course of this work. The authors would also like to thank R. Signell for his assistance and expertise with the Blumberg–Mellor model, and A. Blumberg for permission to use the model code. This work was supported by Gulf of Maine Regional Marine Research Program Grant UM-S227 and Office of Naval Research Grant N00014-01-1-0200. DAF also acknowledges the support of OCE-9907110 and ONR-N00014-98-1-0785.

REFERENCES

- Beardsley R. C., and W. C. Boicourt, 1981: On estuarine and continental-shelf circulation in the Middle Atlantic Bight. *Evolution of Physical Oceanography*, B. A. Warren and C. Wunsch, Eds., The MIT Press, 198–233.
- Blanton J. O., and L. P. Atkinson, 1983: Transport and fate of river discharge on the continental shelf of the southeastern United States. *J. Geophys. Res.*, **88**, 4730–4738. [Find this article online](#)
- Blumberg A. F., and G. L. Mellor, 1987: A description of a three-dimensional coastal ocean circulation model. *Three-Dimensional Coastal Ocean Models*, N. Heaps, Ed., Amer. Geophys. Union, 1–16.
- Boicourt W. C., 1973: The circulation of water on the continental shelf from Chesapeake Bay to Cape Hatteras. Ph.D. thesis, The Johns Hopkins University, 183 pp.
- Brink K. H., 1986: Topographic drag due to barotropic flow over the continental shelf and slope. *J. Phys. Oceanogr.*, **16**, 2152–2158. [Find this article online](#)
- Brink K. H., D. Halpern, and R. L. Smith, 1980: Circulation in the Peruvian upwelling system near 15 degrees South. *J. Geophys. Res.*, **85**, 4036–4048. [Find this article online](#)

- Chao S-Y., 1998: Hyperpycnal and buoyant plumes from a sediment-laden river. *J. Geophys. Res.*, **103**, 3067–3081. [Find this article online](#)
- Chao S-Y., and W. C. Boicourt, 1986: Onset of estuarine plumes. *J. Phys. Oceanogr.*, **16**, 2137–2149. [Find this article online](#)
- Chapman D. C., and S. J. Lentz, 1994: Trapping of a coastal density front by the bottom boundary layer. *J. Phys. Oceanogr.*, **24**, 1464–1479. [Find this article online](#)
- Fong D. A., and W. R. Geyer, 2001: Response of a river plume during an upwelling favorable wind event. *J. Geophys. Res.*, **106**, 1067–1084. [Find this article online](#)
- Fong D. A., W. R. Geyer, and R. P. Signell, 1997: The wind-forced response of a buoyant coastal current: Observations of the western Gulf of Maine plume. *J. Mar. Syst.*, **12**, 69–81. [Find this article online](#)
- Garvine R. W., 1995: A dynamical system of classifying buoyant coastal discharges. *Contin. Shelf Res.*, **15**, 1585–1596. [Find this article online](#)
- Garvine R. W., 1996: Bouyant discharge on the inner continental shelf: A frontal model. *J. Mar. Res.*, **54**, 1–33. [Find this article online](#)
- Garvine R. W., 2001: Artifacts in buoyant coastal discharge models: An observational and model study. *J. Mar. Res.*, **59**, 193–225. [Find this article online](#)
- Griffiths R. W., and E. J. Hopfinger, 1983: Gravity currents moving along a lateral boundary in a rotating fluid. *J. Fluid Mech.*, **134**, 357–399. [Find this article online](#)
- Haidvogel D. B., and K. H. Brink, 1986: Mean currents driven by topographic drag over the continental shelf and slope. *J. Phys. Oceanogr.*, **16**, 2159–2171. [Find this article online](#)
- Hickey B. M., L. J. Pietrafesa, D. A. Jay, and W. C. Boicourt, 1998: The Columbia River plume study: Subtidal variability in the velocity and salinity fields. *J. Geophys. Res.*, **103**, 10339–10368. [Find this article online](#)
- Holloway G., K. Brink, and D. Haidvogel, 1989: Topographic stress in coastal circulation dynamics. *Poleward*, S. J. Neshyba et al., Eds., Springer-Verlag, 315–330.
- Kao T. W., 1981: The dynamics of oceanic fronts. Part II: Shelf water structure due to freshwater discharge. *J. Phys. Oceanogr.*, **11**, 1215–1223. [Find this article online](#)
- Kourafalou V. H., L.-Y. Oey, J. D. Wang, and T. N. Lee, 1996: The fate of river discharge on the continental shelf. 1. Modeling the river plume and the inner shelf coastal current. *J. Geophys. Res.*, **101**, 3415–3434. [Find this article online](#)
- Kundu P. K., and J. S. Allen, 1976: Some three-dimensional characteristics of low-frequency current fluctuations near the Oregon coast. *J. Phys. Oceanogr.*, **6**, 181–199. [Find this article online](#)
- Lentz S. J., and R. Limeburner, 1995: The Amazon River plume during AMASSEDS: Spatial characteristics and salinity variability. *J. Geophys. Res.*, **100**, 2355–2375. [Find this article online](#)
- Marmorino G. O., and C. L. Trump, 2000: Gravity current structure of the Chesapeake Bay outflow plume. *J. Geophys. Res.*, **105**, 28847–28861. [Find this article online](#)
- Marmorino G. O., L. K. Shay, B. K. Haus, R. A. Handler, H. C. Gruber, and M. P. Horne, 1999: An EOF analysis of HF Doppler radar current measurements of the Chesapeake Bay buoyant outflow. *Contin. Shelf Res.*, **19**, 271–288. [Find this article online](#)
- Marmorino G. O., T. F. Donato, M. A. Sletten, and C. L. Trump, 2000: Observations of an inshore front associated with the Chesapeake Bay outflow plume. *Contin. Shelf Res.*, **20**, 665–684. [Find this article online](#)
- Masse A. K., and C. R. Murthy, 1992: Analysis of the Niagara River plume dynamics. *J. Geophys. Res.*, **97**, 2403–2420. [Find this article online](#)
- McCreary J. P., S. Zhang, and S. R. Shetye, 1997: Coastal circulations driven by river outflow in a variable-density 1 1/2-layer model. *J. Geophys. Res.*, **102**, 15535–15554. [Find this article online](#)
- Mellor G. L., and T. Yamada, 1982: Development of a turbulence closure model for geophysical fluid problems. *Rev. Geophys. Space Phys.*, **20**, 851–875. [Find this article online](#)
- Münchow A., and R. W. Garvine, 1993a: Buoyancy and wind forcing of a coastal current. *J. Mar. Res.*, **51**, 293–322. [Find this article online](#)
- Münchow A., and R. W. Garvine, 1993b: Dynamical properties of a buoyancy-driven coastal current. *J. Geophys. Res.*, **98**, 20063–20077.

Nof D., 1988: Eddy-wall interactions. *J. Mar. Res.*, **46**, 527–555. [Find this article online](#)

Oey L.-Y., and G. L. Mellor, 1993: Subtidal variability of estuarine outflow, plume, and coastal current: A model study. *J. Phys. Oceanogr.*, **23**, 164–171. [Find this article online](#)

Pichevin T., and D. Nof, 1997: The momentum imbalance paradox. *Tellus*, **49A**, 298–319. [Find this article online](#)

Rennie S. E., J. L. Largier, and S. J. Lentz, 1999: Observations of a pulsed buoyancy current downstream of Chesapeake Bay. *J. Geophys. Res.*, **104**, 18227–18240. [Find this article online](#)

Smolarkiewicz P. K., and W. W. Grabowski, 1990: The multidimensional positive definite advection transport algorithm. *J. Comput. Phys.*, **86**, 355–375. [Find this article online](#)

Stern M. E., J. A. Whitehead, and B.-L. Hua, 1982: The intrusion of a density current along the coast of a rotating fluid. *J. Fluid Mech.*, **123**, 237–265. [Find this article online](#)

Valle-Levinson A., J. M. Klinck, and G. H. Wheless, 1996: Inflows/outflows at the transition between a coastal plain estuary and the coastal ocean. *Contin. Shelf Res.*, **16**, 1819–1847. [Find this article online](#)

Whitehead J. A., and D. C. Chapman, 1986: Laboratory observations of a gravity current on a sloping bottom: The generation of shelf waves. *J. Fluid Mech.*, **172**, 373–399. [Find this article online](#)

Yankovsky A. E., and D. C. Chapman, 1997: A simple theory for the fate of buoyant coastal discharges. *J. Phys. Oceanogr.*, **27**, 1386–1401. [Find this article online](#)

Zhang Q. H., G. S. Janowitz, and L. J. Pietrafesa, 1987: The interaction of estuarine and shelf waters: A model and applications. *J. Phys. Oceanogr.*, **17**, 455–469. [Find this article online](#)

Tables

TABLE 1. Parameters of numerical calculations presented in section 6: Q_r is the total volumetric transport of the river discharge, Q_{fr} is the freshwater river discharge, and $(\Delta S)_r$ is the salinity anomaly associated with the river discharge. All other variables are defined in the text

Run	Q_r ($\text{m}^3 \text{s}^{-1}$)	Q_{fr} ($\text{m}^3 \text{s}^{-1}$)	$(\Delta S)_r$ (psu)	$(\Delta \rho)_r$ (kg m^{-3})	h_r (m)	L_r (km)
1	10 000	1250	4	3.1	15	3
2	10 000	1250	4	3.1	15	6
3	10 000	1250	4	3.1	15	9
4	10 000	1250	4	3.1	15	12
5	10 000	1250	4	3.1	3	3
6	10 000	1250	4	3.1	3	6
7	10 000	1250	4	3.1	3	9
8	10 000	1250	4	3.1	3	12
9	10 000	1250	4	3.1	3	15
10	10 000	1250	4	3.1	30	3
11	10 000	1250	4	3.1	30	9
12	10 000	1250	4	3.1	30	15
13	5000	1250	8	6.2	15	3
14	2500	1250	16	12.4	15	3
15	10 000	1250	4	3.1	15	3
16	10 000	1250	4	3.1	15	3

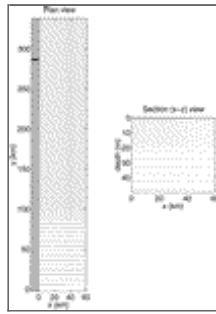
[Click on thumbnail for full-sized image.](#)

TABLE 2. Summary of freshwater transport at $t = 5$ days, $y = 252$ km for different model runs presented in section 3. The Rossby number $Ro = u_r/fL_r$ is shown

Run	L_r (km)	u_r (m s^{-1})	Ro	Q_{oc} ($\text{m}^3 \text{s}^{-1}$)
1	3	0.22	0.74	594
2	6	0.11	0.19	761
3	9	0.07	0.08	808
4	12	0.06	0.04	838
5	3	1.11	3.70	290
6	6	0.56	0.93	570
7	9	0.37	0.41	587
8	12	0.28	0.23	687
9	15	0.22	0.15	769
10	3	0.11	0.37	675
11	9	0.04	0.04	865
12	15	0.02	0.01	913
13	3	0.11	0.37	708
14	3	0.06	0.19	752
15	3	0.22	1.48	594
16	3	0.22	2.96	594

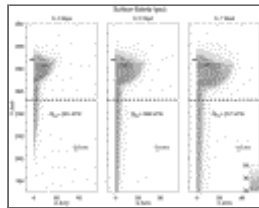
[Click on thumbnail for full-sized image.](#)

Figures



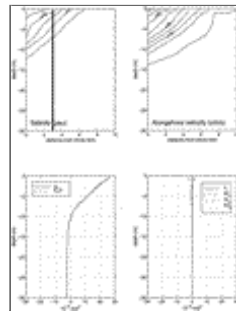
[Click on thumbnail for full-sized image.](#)

FIG. 1. Model configuration. [Blumberg and Mellor's \(1987\)](#) ECOM-3D is run on a $65 \text{ km} \times 340 \text{ km} \times 50 \text{ m}$ grid. Grid resolution is indicated by small dots in both plan and section views. Vertical sigma levels are closely spaced at the surface to resolve the near-surface plume behavior. Freshwater is discharged from a river at $x = 0$ centered about the alongshore position $y = 287.5 \text{ km}$ (indicated by arrow). The river width is varied from 3 to 15 km [in vicinity of river mouth, grid cells (dots) are spaced 3 km apart in the alongshore (y) direction]. The coastline (and land) is shaded in light gray



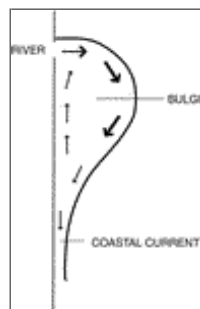
[Click on thumbnail for full-sized image.](#)

FIG. 2. Surface salinity (psu), indicated by gray shading, for the base case model run (run 1) at $t = 3, 5,$ and 7 days. Velocity vectors are superimposed to indicate the flow field. Freshwater transport in the coastal current is measured at $y = 252 \text{ km}$ (indicated by dashed line). River mouth location is indicated by bold arrow



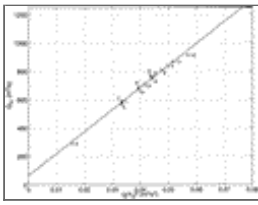
[Click on thumbnail for full-sized image.](#)

FIG. 3. Sections of salinity (psu) and alongshore velocity are shown in the upper two panels. Profiles of terms in the cross-shore momentum balance are shown in the lower panels at the location given by the heavy vertical line overlying the salinity contours




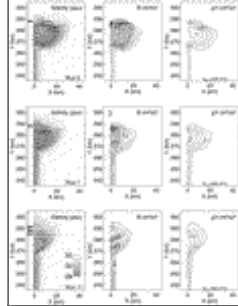
[Click on thumbnail for full-sized image.](#)

FIG. 4. Cartoon of circulation within a bulge and coastal current. The flow along the seaward side of the bulge transports water that supplies both the coastal current and the continually growing recirculation within the bulge



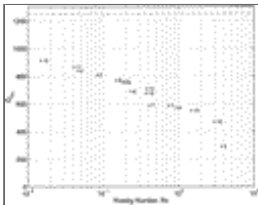
Click on thumbnail for full-sized image.

FIG. 5. Model freshwater transport Q_{fcc} in a coastal current at $t = 5$ days, $y = 252$ km as a function squared potential energy in coastal current. Run numbers are indicated for each data point (see [Table 2](#) )



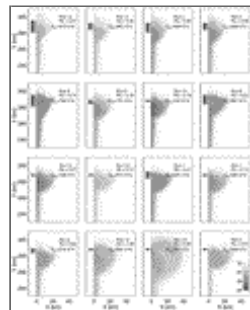
Click on thumbnail for full-sized image.

FIG. 6. Bulge behavior for different inflow conditions. The surface salinity and velocity, Bernoulli function B , and potential energy $g' h$ are plotted for runs 5, 1, and 11. Shaded regions in the panels plotting B and $g' h$ indicate regions of B and $g' h > 0.279 \text{ m}^2 \text{ s}^{-2}$. Contours of B and $g' h$ are in intervals of $0.05 \text{ m}^2 \text{ s}^{-2}$. The coastal current transport at $y = 252$ km is shown in the lower right of the $g' h$ contours.



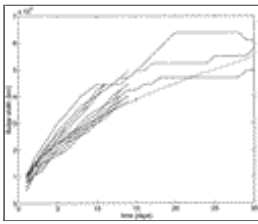
Click on thumbnail for full-sized image.

FIG. 7. Freshwater transport ($\text{m}^3 \text{ s}^{-1}$) as a function of Rossby number at $t = 5$ days, $y = 252$ km. For runs 15 and 16, the transport is calculated at $y = 232$, an alongshore position outside of the bulge. The dashed line indicates the freshwater discharge rate at the river mouth



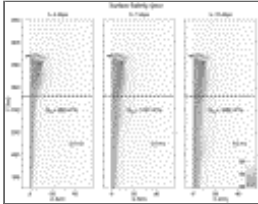
Click on thumbnail for full-sized image.

FIG. 8. Surface salinities at $t = 5$ days for different Rossby number conditions are shown in gray. Locations of the river mouth (and river widths) are indicated by the arrows. The width of the river mouth is the number of arrows times 3 km (e.g., the river mouth is 15 km wide for run 12). The Rossby number and the freshwater transport in the coastal current (at $y = 252$ km for runs 1–14 and $y = 232$ km for runs 15 and 16) are shown in each panel.



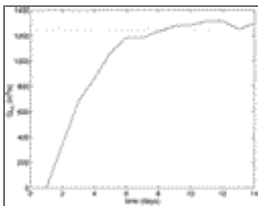
[Click on thumbnail for full-sized image.](#)

FIG. 9. Bulge width (defined by the position of the 31.5-psu isohaline) as a function of time for different model runs. The bulge width is approximately proportional to the square root of time for the different model runs (the dotted line denotes a $t^{1/2}$ dependence). Note: bulge widths for $t > 20$ days may not be accurate due to interactions of the bulge with the offshore boundary of the model domain



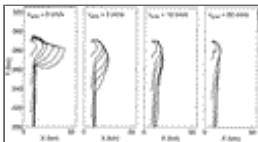
[Click on thumbnail for full-sized image.](#)

FIG. 10. Surface salinity (psu) indicated by gray shading for an ambient current of 10 cm s^{-1} but otherwise the same conditions as the base case ($t = 4, 7, 10$ days). Velocity vectors are superimposed to indicate the flow field. Freshwater transport is measured at $y = 252$ km (indicated by dashed line). River mouth location is indicated by bold arrow



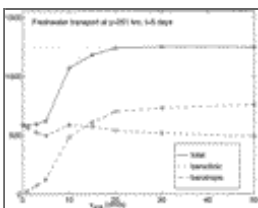
[Click on thumbnail for full-sized image.](#)

FIG. 11. Freshwater transport ($\text{m}^3 \text{ s}^{-1}$) as a function of time at $y = 252$ km for same parameters as the base case plus an ambient flow field of 10 cm s^{-1} southward. The dotted line indicates the freshwater discharge by the river: $1250 \text{ m}^3 \text{ s}^{-1}$



[Click on thumbnail for full-sized image.](#)

FIG. 12. Traces of 31-psu isohaline at plume surface ($z = 0$) for the base case with different ambient flow fields. Traces are for $t = 1, 3, 5, 7,$ and 9 days



[Click on thumbnail for full-sized image.](#)

FIG. 13. Freshwater transport as a function of ambient flow field strength at $y = 252$ km at $t = 5$ days. The baroclinic transport is plotted with a dashed line, the barotropic transport with a dash-dot line, and the sum with a solid line. The dotted line indicates the rate of freshwater discharge by the river, $1250 \text{ m}^3 \text{ s}^{-1}$

* Woods Hole Oceanographic Institution Contribution Number 10494.

Corresponding author address: Dr. Derek A. Fong, Environmental Fluid Mechanics Laboratory, Dept. of Civil and Environmental Engineering, Stanford University, Stanford, CA 94305-4020. E-mail: dfong@stanford.edu

top ▲



© 2008 American Meteorological Society [Privacy Policy and Disclaimer](#)

Headquarters: 45 Beacon Street Boston, MA 02108-3693

DC Office: 1120 G Street, NW, Suite 800 Washington DC, 20005-3826

amsinfo@ametsoc.org Phone: 617-227-2425 Fax: 617-742-8718

[Allen Press, Inc.](#) assists in the online publication of *AMS* journals.